



Cite this: *Phys. Chem. Chem. Phys.*,  
2014, 16, 25024

# Spectroscopic investigation of the binding interactions of a membrane potential molecule in various supramolecular confined environments: contrasting behavior of surfactant molecules in relocation or release of the probe between nanocarriers and DNA surface†

Surajit Ghosh, Debasis Banik, Arpita Roy, Niloy Kundu, Jagannath Kuchlyan and Nilmoni Sarkar\*

The fluorescence and optical properties of membrane potential probes are widely used to measure cellular transmembrane potentials. Hemicyanine dyes are also able to bind to membranes. The spectral properties of these molecules depend upon the charge shift from the donor moiety to the acceptor moiety. Changes in their spectral properties, *i.e.* absorption and emission maxima or intensities, are helpful in characterizing model membranes, microheterogeneous media, etc. In this article, we have demonstrated the binding interaction of a membrane potential probe, 1-ethyl-2-(4-(*p*-dimethylaminophenyl)-1,3-butadienyl)-pyridinium perchlorate (LDS 698), with various supramolecular confined environments. The larger dipole moment in the ground state compared to the excited state is a unique feature of hemicyanine dyes. Due to this unique feature, red shifts in the absorption maxima are observed in hydrophobic environments, compared with bulk solvent. On addition of surfactants and CT DNA to an aqueous solution containing LDS 698, significant increase in the emission intensity along with the quantum yield and lifetime indicate partition of the probe molecules into organized assemblies. In the case of the sodium dodecyl sulfate (SDS)-water system, due to interactions between the cationic LDS 698 and the anionic dodecyl sulfate moiety, the fluorescence intensity at ~666 nm decreases and an additional peak at ~590 nm appears at premicellar concentration (~0.20 mM–4.50 mM). But at ~5.50 mM SDS concentration, the absorbance in the higher wavelength region increases again, indicating encapsulation of the probe in micellar aggregates. This observation indicates that the premicellar aggregation behavior of SDS can also be judged by observing the changes in the UV-vis and fluorescence spectral patterns. The temperature dependent study also indicates that non-radiative deactivation of the dye molecules is highly restricted in the DNA micro-environment, compared with micelles. Besides, we have also investigated the specific interaction of surfactant micelles with DNA. Our observations reveal that, in the presence of CT DNA, LDS 698 interacts exclusively with SDS micelles, but that it preferentially releases from micelles and relocates to DNA surfaces in solutions containing TX-100 micelles.

Received 18th July 2014,  
Accepted 4th October 2014

DOI: 10.1039/c4cp03178d

[www.rsc.org/pccp](http://www.rsc.org/pccp)

## 1. Introduction

Hemicyanine molecules, featuring an electron donor and an acceptor moiety in conjugation, are pharmaceutically important due to their ability to detect changes in membrane voltage in neurons,<sup>1,2</sup> and also used as frequency converters,<sup>3,4</sup>

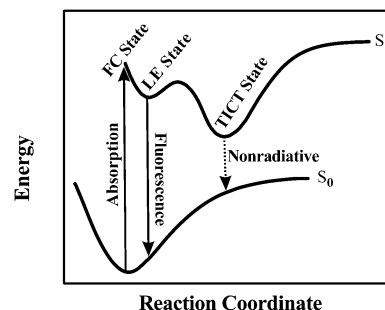
fluorescence markers,<sup>5</sup> *etc.* During photo-excitation, internal rotation between the amine group and the pyridinium moiety creates the possibility of a twisted intramolecular charge transfer (TICT) state.<sup>6,7</sup> The intramolecular rotational motion of hemicyanine molecules is mainly dependent on the solvent viscosity and polarity.<sup>8</sup> Depending on substitution at the electron donor or electron acceptor group, hemicyanine dyes exhibit variation in their photoinduced intramolecular charge transfer processes.<sup>9</sup> The important feature of the TICT state is the dual fluorescence in polar solvents.<sup>10</sup> McHale *et al.* showed the existence of the TICT state in hemicyanine dyes, and its non-radiative decay channel was confirmed using ultra-fast resonance Raman spectroscopy

Department of Chemistry, Indian Institute of Technology, Kharagpur 721302, WB, India. E-mail: nilmoni@chem.iitkgp.ernet.in; Fax: +91-3222-255303

† Electronic supplementary information (ESI) available: Information on the circular dichroism (CD), variation of the non-radiative rate constant, and temperature dependent UV-vis and fluorescence spectra of LDS in micelles and DNA solution. See DOI: 10.1039/c4cp03178d

and theoretical studies.<sup>11,12</sup> The quantum yields of hemicyanine dyes in homogenous solvent are very low due to deactivation through bond twisting processes in the excited state.<sup>13–15</sup> Researchers are presently interested in investigating the structural and photophysical aspects of molecules entrapped in protein environments, DNA surfaces, micelles, reverse micelles, vesicles or various nanocavities due to the promising effects of confined assemblies on photophysical and biological phenomena.<sup>16–27</sup> Compared with pure solvent, these microheterogeneous media can provide different environments (microviscosity, micropolarity, *etc.*) to solute molecules.

The binding of deoxyribonucleic acid (DNA) with various small molecules is an attractive topic to researchers, as it provides necessary information regarding the structural aspects and therapeutic applications of DNA. The sensitivity of fluorescent compounds makes fluorescence an efficient tool for observing the binding affinity, structural information, *etc.*<sup>28–37</sup> During the drug–DNA binding process, drug molecules can bind to three different sites *via* electrostatic or hydrophobic interactions. The three binding modes are: (i) incorporation within a DNA base pair, *i.e.*, an intercalative mode of binding, (ii) major or minor groove binding through van der Waal's interactions, and (iii) binding between the negatively charged phosphate backbone and the cationic end of the drug molecule *via* attractive electrostatic interactions. During groove binding, drug molecules are accommodated inside the DNA grooves, but in the intercalation process, planar aromatic drug molecules insert between the base pairs of DNA molecules.<sup>25,38–40</sup> The interactions between DNA and small molecules, including several drugs, are well reported in the literature.<sup>40–44</sup> However, controlled switching of drug molecules between DNA surfaces and different drug carriers is still an interesting research topic. We have focused on surfactant micelles as a model carrier. Micelles, supramolecular assemblies of surfactant molecules, are sometimes used as model carrier systems, as they can accommodate probe molecules very efficiently. Weak hydrophobic interactions between surfactant molecules lead to the formation of spherical aggregates called micelles in aqueous medium. Theoretical and experimental studies revealed that water molecules bound to DNA show similar characteristics to water molecules bound to micelles.<sup>45–51</sup> DNA, a cylindrical polyelectrolyte, contains a negatively charged phosphate backbone and a hydrophobic interior with nitrogen base pairs. Similarly, micelles are spherical polyelectrolytes with a charged surface and a hydrophobic core.<sup>52</sup> The structural similarities between these assemblies caused researchers to become interested in studying their reversible binding patterns. Therefore, it is interesting to study the interaction pattern of LDS 698 with CT DNA in the presence of surfactant micelles. Controlled release of thioflavin T (ThT) from SDS micelles to CT DNA molecules using beta cyclodextrin ( $\beta$ -CD) as an external agent has been recently shown.<sup>53</sup> Mitra and co-workers have determined various energetic parameters for the deintercalation of phenosafranine (PSF) between SDS micelles and DNA molecules.<sup>54</sup> Here, we are interested in visualizing the effect of the surface charge of surfactant micelles on the binding of dye molecules in the presence of CT DNA.



Scheme 1 Schematic representation of the potential energy surface.  $S_1$ : singlet excited state;  $S_0$ : ground state; LE: local excited state; FC: Franck–Condon state; and TICT: twisted intramolecular charge transfer state.

1-Ethyl-2-(4-(*p*-dimethylaminophenyl)-1,3-butadienyl)-pyridinium perchlorate, LDS 698, is used as a probe molecule in our experiments. The solvent dependent radiative and non-radiative processes of LDS 698 have been investigated in various alcohols, water–dioxane binary solutions and room temperature ionic liquids (RTILs).<sup>13</sup> The photophysical properties of various hemicyanine dyes in homogenous solvent, organized media and ionic liquids are well documented.<sup>13,55–58</sup> Based on the photophysical aspects, a simplified model (Scheme 1) was introduced to explain the excited state dynamics of LDS 698 molecules.<sup>56,59,60</sup>

In this manuscript, we have investigated the photophysical properties of a hemicyanine dye (LDS 698) in micellar nanocavities with different surface charges and DNA surfaces. The presence of the charged pyridinium moiety decreases its solubility in non-polar solvents, whereas the long alkyl part increases its solubility in these solvents. It was observed that this dye is insoluble in *n*-heptane and completely soluble in water. But the presence of an inherent hydrophobic environment within the micellar systems compelled us to investigate the partition of LDS 698 in this environment. We also investigated micelle-induced localization or delocalization of dye molecules on DNA surfaces. Three surfactants, SDS, CTAB and TX-100, were used to visualize this phenomenon. Circular dichroism spectroscopy, steady state and time resolved fluorescence measurements are also able to provide structural information on the binding environment of DNA in the presence of surfactant micelles. The structural changes of DNA molecules in the presence of cationic surfactants are a well documented phenomenon. The hydrophobic and attractive interactions between the cationic surfactant and the negatively charged DNA molecules lead to phase separation, which is indicative of the conformational changes of DNA in solution, and is useful for the purification of DNA and other biomedical processes.<sup>61–67</sup> But we are interested in observing the switching of probe molecules between nanocarriers and DNA surfaces. Circular dichroism spectroscopy was used to observe the conformation of DNA in the presence of surfactant molecules. We used steady state and time resolved fluorescence spectroscopic techniques to observe the binding behavior of a membrane potential molecule, 1-ethyl-2-(4-(*p*-dimethylaminophenyl)-1,3-butadienyl)-pyridinium perchlorate (LDS 698) in TX-100 and SDS micelles in the presence of CT DNA in aqueous buffer solution.

## 2. Experimental section

### 2.1. Materials

1-Ethyl-2-(4-(*p*-dimethylaminophenyl)-1,3-butadienyl)-pyridinium perchlorate, (LDS 698) (laser grade, Exciton) was used as received. Cetyltrimethyl ammonium bromide (CTAB) and Triton X-100 (TX-100) were purchased from Sigma Aldrich, and sodium dodecyl sulfate (SDS), the sodium salt of deoxyribonucleic acid (Calf Thymus DNA, CT DNA) and Tris-buffer were purchased from Sisco Research Chemical Laboratory (SRL), India. All these materials were used as received without further purification. Triply distilled Milli-Q water was used to prepare all solutions. The purity of the CT DNA was verified using an absorption spectrometer. The optical density ratio of the absorption bands of CT DNA at 260 nm and 280 nm was found to be 1.8–1.85. To prepare the homogenous aqueous solutions, solid CT DNA was added to Tris-HCl buffer (pH ~ 7.4, 0.01 M) and kept at 4 °C for 2 days with occasional shaking using mild sonication. The structures of all the chemicals used in this experiment are shown in Scheme 2.

### 2.2. Instruments and method

The UV-vis absorption and fluorescence spectra were acquired using a Shimadzu (model no. UV-2405) spectrophotometer and a Hitachi (model no. F-7000) spectrofluorimeter, respectively. Circular dichroism (CD) spectra were recorded using a JASCO (J-815) CD spectrometer with a quartz cuvette and a 10 mm path length.

The time resolved emission spectra were obtained using a time correlated single photon counting (TCSPC) setup with a picosecond diode pulsed 408 nm laser as excitation source. In brief, emission decays were collected at the respective emission maxima of the solutions using a Hamamatsu MCP PMT (3809U) with an emission polarizer at the magic angle (54.7°). The instrumental resolution of our TCSPC set up is ~ 90 ps. The decays were analyzed with the help

of IBH DAS-6 decay analysis software. The temperature was maintained using a circulating water bath.

We used coumarin-480 (C 480) in water as a reference, and the following equation was used for the calculation of the quantum yield.<sup>68,69</sup>

$$\Phi_{\text{Sample}} = \Phi_{\text{Reference}} \times \frac{A_{\text{Sample}}}{A_{\text{Reference}}} \times \frac{(\text{Abs})_{\text{Reference}}}{(\text{Abs})_{\text{Sample}}} \times \frac{n_{\text{Sample}}^2}{n_{\text{Reference}}^2} \quad (1)$$

Here, ‘Φ’, ‘Abs’, ‘A’ and ‘n’ represent quantum yield, absorbance, area under the fluorescence curve, and refractive index of the medium, respectively.

The time resolved decay curves for the lifetime measurements were fitted using the following exponential function:<sup>69</sup>

$$I(t) = \sum_i a_i e^{-t/\tau_i} \quad (2)$$

where  $a_i$  and  $\tau_i$  represent the pre-exponential factor and lifetime of the  $i$ th component, respectively.

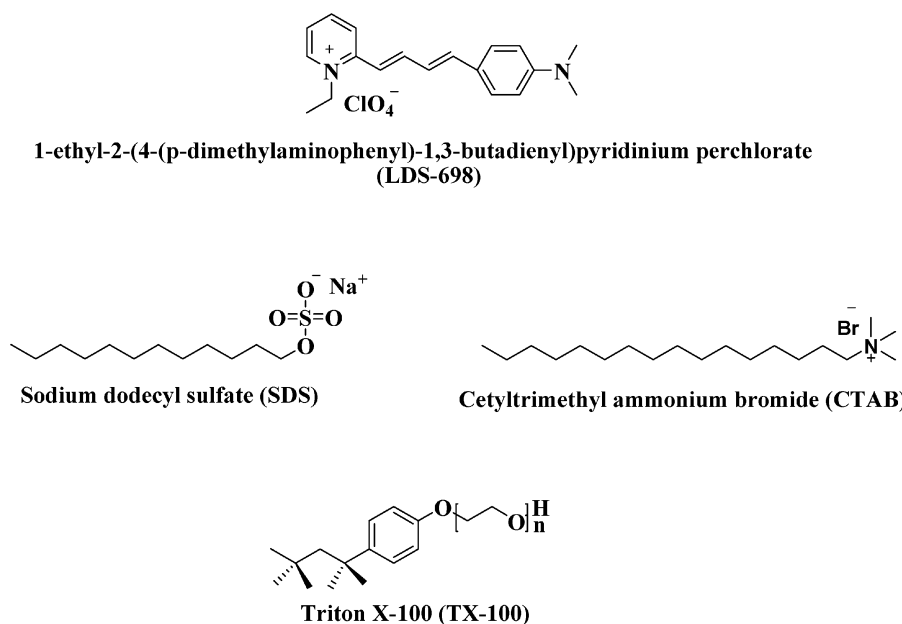
The average fluorescence lifetime was calculated using the following equation:<sup>69</sup>

$$\langle \tau_{\text{av}} \rangle = \sum_i a_i \tau_i \quad (3)$$

## 3. Results and discussion

### 3.1. Circular dichroism (CD) measurements

The circular dichroism (CD) study allowed us to obtain information regarding the conformational changes of DNA molecules. In order to understand the structural aspects of DNA molecules in the presence of LDS 698 and surfactant molecules (SDS, CTAB, and TX-100), CD spectra of CT DNA were recorded



**Scheme 2** Structures of the fluorescence probe: 1-ethyl-2-(4-(*p*-dimethylaminophenyl)-1,3-butadienyl)-pyridinium perchlorate (LDS 698); and the surfactants: sodium dodecyl sulfate (SDS), cetyltrimethyl ammonium bromide (CTAB) and Triton X-100 (TX-100).

in Tris-buffer at pH = ~7.4, and are shown in Fig. S1 (ESI<sup>†</sup>). The CD spectrum of CT DNA in aqueous Tris-buffer displays a positive band at approximately 280 nm and a negative band at approximately 245 nm, which is characteristic of the B-form of DNA in aqueous solution.<sup>70</sup> On increasing the concentration of LDS 698, the enhancement in the band intensity is negligible (Fig. S1a, ESI<sup>†</sup>). The CD spectrum indicates that the binding of the probe to CT DNA does not disturb the secondary structure of DNA. A slight variation in the CD signal at ~475–477 nm is observed on increasing the LDS 698 concentration (Fig. S1b, ESI<sup>†</sup>). Achiral molecules do not show any CD signal in aqueous buffer solution, but an induced CD signal can be observed upon binding to DNA. The signal depends upon the binding mode, depth of intercalation, orientation of the transition dipoles, etc.<sup>71</sup> However, in our study in CT DNA solution, the enhancement in the induced CD signal with increasing concentration of LDS 698 is also negligible. Therefore, these observations rule out intercalation of LDS 698 in the DNA helix, and indicate that the probe molecule binds to the DNA through groove binding or electrostatic interactions.

The interaction pattern of surfactant molecules with DNA mainly depends on the surface charge of the surfactant molecules. The structural change of DNA in the presence of cationic surfactant molecules has been investigated extensively.<sup>61–64</sup> After addition of a cationic surfactant, DNA molecules compact and form a globule state. Above a certain concentration, the surfactant molecules form micellar assemblies at the surface of the nucleic acid. This micellar nanostructure acts as a multi-valent ion and induces DNA compaction. In our study, we also monitored the CD spectra of DNA in the presence of increasing concentrations of surfactants with different surface charges (Fig. S1c–e, ESI<sup>†</sup>). In the case of anionic surfactant assemblies, the close approach of DNA and SDS micelles is inhibited due to repulsive interactions between the head group of SDS and the negatively charged DNA. As a result, the CD spectra of CT DNA in the presence of SDS solution remain almost unchanged. Therefore, the conformation of the DNA molecules remains unaltered in the presence of anionic micellar assemblies. Similarly, we recorded CD spectra of CT DNA in the presence of TX-100 solution. But the changes observed below 250 nm in the CD spectra of DNA suggest that the secondary structure of the DNA molecules is affected by the presence of TX-100. TX-100 molecules contain an aromatic ring; therefore, this observed change may occur due to pi-pi interactions between the aromatic ring of the surfactant and the nitrogen bases. But it is important to note that self absorption of TX-100 molecules can also induce this deviation in the CD spectra.

### 3.2. Steady state UV-vis and fluorescence studies

**3.2.1. Encapsulation of LDS 698 in surfactant micelles.** The UV-vis absorption spectra of LDS 698 in water and 100 mM CTAB, SDS, and TX-100 solutions are shown in Fig. 1. Generally, dye molecules exhibit a blue shift in the absorption spectrum with the addition of surfactant molecules in aqueous solution. But the blue shifts in the absorption maxima of hemicyanine dye molecules in polar media indicate that the dipole moment

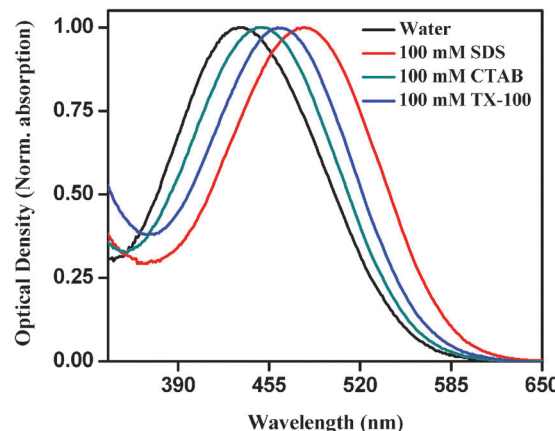


Fig. 1 UV-visible absorption spectra of LDS 698 in water, and in 100 mM SDS, CTAB and TX-100 solutions.

Table 1 Absorption and emission maxima of LDS 698 in different micellar solutions

System	$\lambda_{\text{abs}}^{\max}$ (nm)	$\lambda_{\text{em}}^{\max}$ (nm)
Water	434	666
100 mM SDS	480	662
100 mM CTAB	448	651
100 mM TX-100	461	648

in the ground state is larger than that in the excited state (Franck-Condon region). The absorption and emission maxima of LDS 698 in water and micelle solutions are provided in Table 1. The absorption band of LDS 698 in water occurs at ~434 nm, whereas it is red shifted to ~480 nm, ~448 nm and ~461 nm in SDS, CTAB and TX-100 solution, respectively. Theoretical analysis revealed that there are two resonance structures for hemicyanine dyes, the benzenoid and the quinoid forms.<sup>12</sup> Generally, the benzenoid form is more stable in polar solvents, whereas the quinoid form is stable in non-polar solvents. Absorption by the benzenoid form occurs at shorter wavelength than absorption by the quinoid form.<sup>72</sup> In micellar solution, the UV-vis spectra were red shifted due to the decrease in micropolarity, *i.e.* the increase in non-polar environment around the probe molecules. The change in the absorption spectrum was found to be greatest in SDS solution and follows the trend: SDS > TX-100 > CTAB. This can be explained by the Coulombic interaction with the surface charge and the hydrophobic interaction of the micelles with the probe molecules. Due to the presence of a negative charge at the surface, solubilization of LDS 698 is greater in SDS than in other micelles.

The anomalous solvatochromism of charged push-pull polyenes (CPPPs) was explained by Hynes and co-workers.<sup>73</sup> During excitation from the electronic ground state to the excited state, charge transfer occurs from one end of these molecules to the other. Therefore, the absorption transition energy ( $E_{\text{abs}}$ ) is related to the adiabatic equilibrium energy gap ( $V_{\text{eq}}^{\text{adia}}$ ) and the adiabatic solvent reorganization energy in the excited state ( $\lambda_s^{\text{ex}}$ ). Similarly, the emission transition energy ( $E_{\text{em}}$ ) is related to the adiabatic equilibrium energy gap ( $V_{\text{eq}}^{\text{adia}}$ )

and the solvent reorganization energy in the adiabatic ground state ( $\lambda_s^g$ ):

$$E_{\text{abs}} = V_{\text{eq}}^{\text{adia}} + \lambda_s^g$$

and

$$E_{\text{em}} = V_{\text{eq}}^{\text{adia}} - \lambda_s^g \quad (4)$$

It has been reported that the sizes of the end groups of hemicyanine dyes are almost identical.<sup>13</sup> Therefore, the electrostatic interaction energy of hemicyanine molecules with different solvents does not depend upon the end group of the molecule. So,  $V_{\text{eq}}^{\text{adia}}$  always remains unaltered with variations in solvent polarity, but  $\lambda_s^g$  and  $\lambda_s^e$  depend on the polarity of the solvent.  $V_{\text{eq}}^{\text{adia}}$  remains almost the same, but both  $\lambda_s^e$  and  $\lambda_s^g$  increase with increasing solvent polarity. So, the above equations suggest that the absorption energy increases and the emission energy decreases with increasing solvent polarity. For this reason, the absorption spectrum of LDS 698 shows a blue shift and the corresponding emission spectrum shows a red shift on moving from a non-polar to a polar medium.

In recent times, fluorescence techniques have been widely used to investigate the binding of probe molecules in different aggregates. Fluorescence spectra of LDS 698 in different micellar systems are depicted in Fig. 2. In aqueous solution, LDS 698 shows an emission maximum at  $\sim 666$  nm, but on gradual addition of surfactants, enhancement in the fluorescence intensity along with a blue shift in the emission maximum was observed (Fig. 3). The enhancement in the emission intensity can be rationalized by entrapment of LDS 698 in micelles. In order to obtain quantitative information on the interaction between LDS 698 and the micellar system, the binding constant was determined using the following method described by Almgren *et al.*<sup>74</sup>

$$\frac{F_\infty - F_0}{F_t - F_0} = 1 + \frac{1}{K[M]} \quad (5)$$

where  $F_0$ ,  $F_t$  and  $F_\infty$  are the fluorescence intensities of LDS 698 in the absence of surfactant, at various concentrations of surfactant, and at the point of saturation, respectively.  $K$  represents the

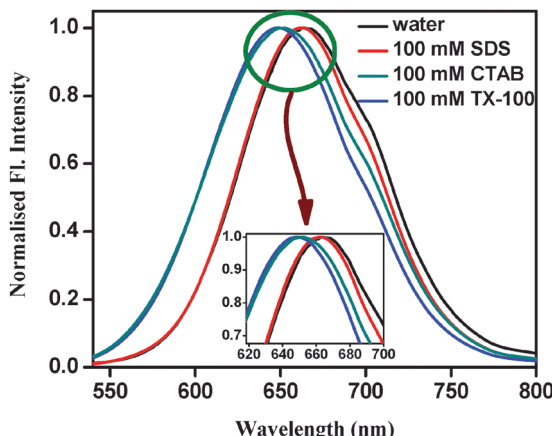


Fig. 2 Emission spectra ( $\lambda_{\text{ex}} = 408$  nm) of LDS 698 in water, and in 100 mM SDS, CTAB and TX-100 solutions.

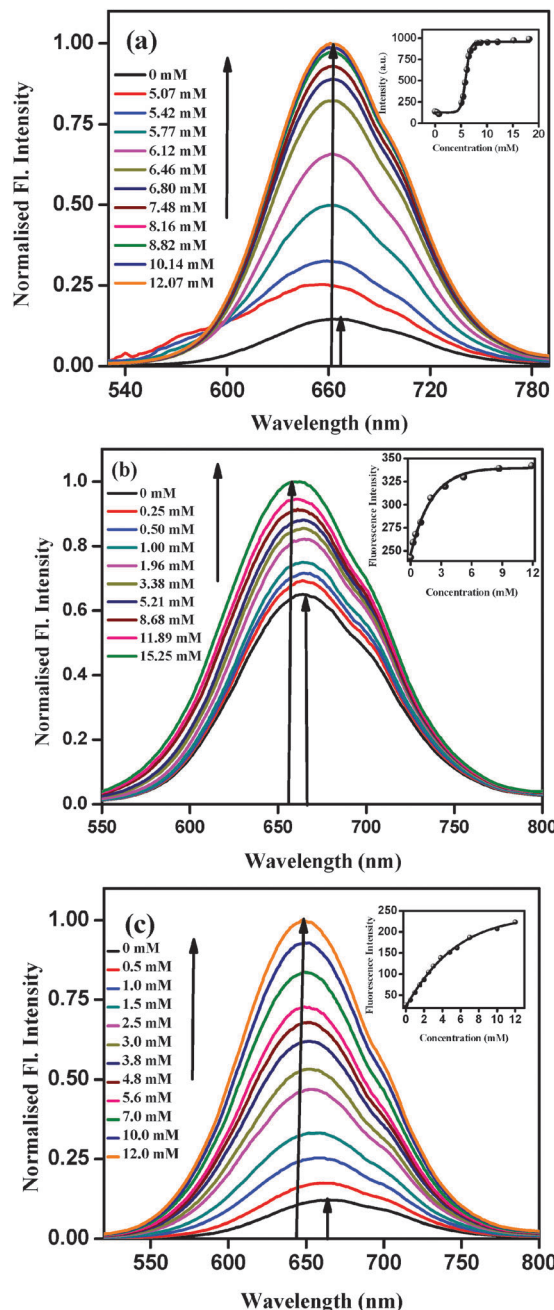


Fig. 3 Emission spectra of LDS-698 ( $\lambda_{\text{ex}} = 408$  nm) in the presence of increasing concentration of surfactant: (a) SDS, (b) CTAB and (c) TX-100.

binding constant between the probe and the micelle.  $[M]$  denotes the concentration of micelles in solution. We calculated  $[M]$  from the surfactant concentration  $[S]$  using the following equation:

$$[M] = \frac{[S] - \text{CMC}}{N_{\text{agg}}} \quad (6)$$

The aggregation values ( $N_{\text{agg}}$ ) of different aqueous surfactant solutions have been reported in the literature.<sup>75,76</sup> The plots of  $(I_\infty - I_0)/(I_t - I_0)$  vs.  $1/[M]$  for SDS, CTAB and TX-100 are shown in Fig. 4. The calculated binding constant values are provided in Table 2. The binding constant values of the micelles follow

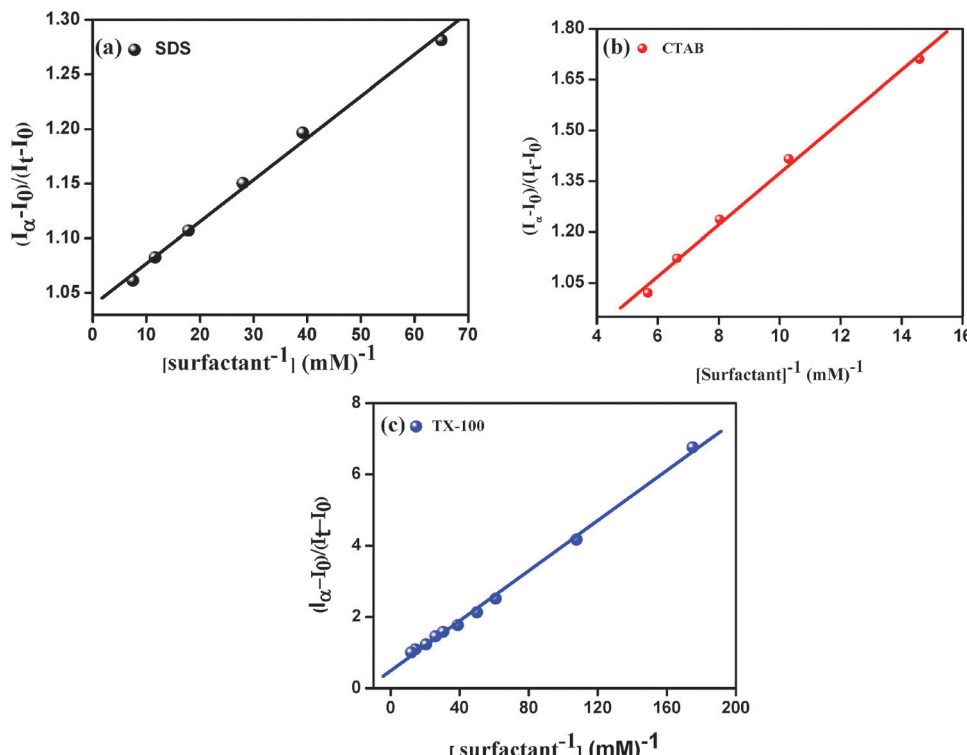


Fig. 4 Plots of  $(I_{\infty} - I_0)/(I_t - I_0)$  vs. (a)  $[\text{SDS}]^{-1}$ , (b)  $[\text{CTAB}]^{-1}$  and (c)  $[\text{TX-100}]^{-1}$ .

Table 2 Binding constants ( $K$ ), for the interaction of LDS 698 with different micelles

Micellar environment	Binding constant/ $K$ ( $10^4 \text{ M}^{-1}$ )
SDS	26.10
CTAB	1.43
TX-100	2.85

the order: SDS > TX-100 > CTAB. In an anionic micellar solution of SDS, LDS 698 experiences greater interactions due to its positive charge. Hence, its binding constant is much higher in SDS than in CTAB or TX-100 solutions. In the non-ionic

micelle, TX-100, the probe molecules experience greater microviscosity due to the very thick palisade layer and the close packing of the surfactant chain. But in CTAB solution, the repulsive interactions between the positive charges reduce the partition of LDS 698 in the CTAB micelle. Hence, the binding constant of LDS 698 is lowest in the CTAB micelle.

LDS 698 shows an absorption band at  $\sim 434 \text{ nm}$  and an emission maximum at  $\sim 666 \text{ nm}$  in aqueous solution, but, on successive addition of SDS to an aqueous solution of LDS 698, significant changes in the spectral profile are observed, as depicted in Fig. 5. At low SDS concentration ( $< 4.5 \text{ mM}$ ), the absorbance and emission intensities at the corresponding peak

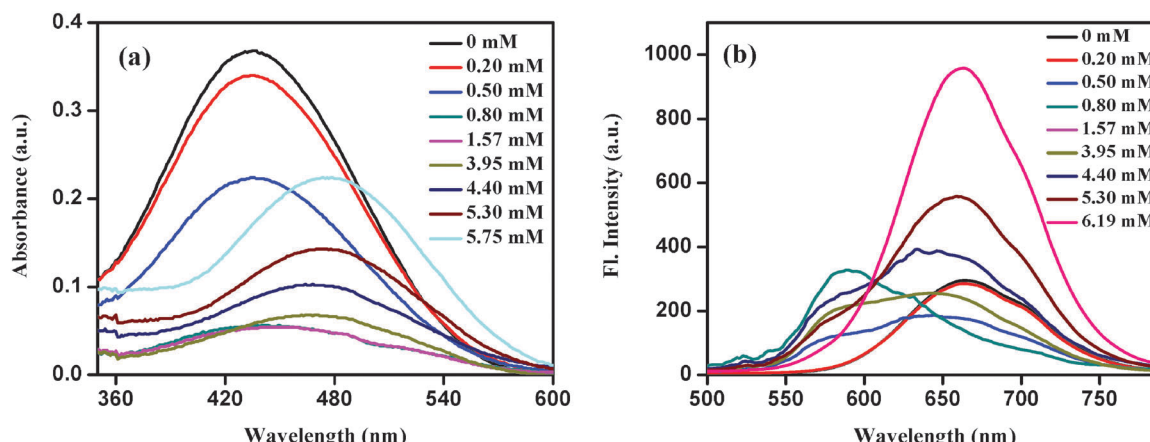


Fig. 5 (a) Absorption and (b) emission spectra ( $\lambda_{\text{ex}} = 408 \text{ nm}$ ) of LDS 698 in water and varying concentrations of SDS.

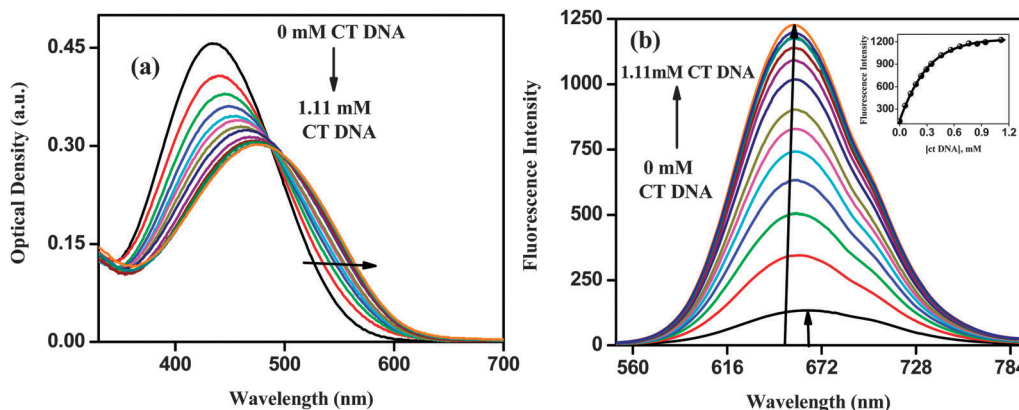


Fig. 6 (a) UV-vis absorption and (b) emission spectra of LDS 698 with increasing concentration of CT DNA.

maxima decrease. These observed changes in the absorbance and emission spectra below the critical micelle concentration (CMC) are due to the formation of complexes between the positively charged LDS 698 and the negatively charged dodecyl sulphate (DS) ions. A new band appears in the emission spectrum at  $\sim 590$  nm. On further addition of SDS, the intensity of the emission peak at  $\sim 590$  nm decreases, and a single peak at  $\sim 662$  nm is observed at concentrations above  $\sim 5.30$  mM. A significant red shift in the absorption spectrum is observed above  $\sim 5.30$  mM, due to encapsulation of the probe in surfactant aggregates.

Cyanine dyes can easily form aggregates in solvents or in confined environments.<sup>56,77–80</sup> These aggregates (J aggregates or H aggregates) can be typically assigned by observing bathochromic or hypsochromic shifts in the absorption spectra in comparison to the monomer band. In the SDS-water system, the spectral shift in the absorption of LDS 698 is negligible at low concentration, and a new band does not appear in the absorption spectrum. Therefore, these aggregates cannot be assigned as J- or H-type. At low concentrations of SDS, a shiny complex (visible) is formed and the solution becomes colourless, due to attractive electrostatic interactions between the probe and SDS. The quantum yield of LDS 698 is very low and the emission spectrum is not smooth after formation of the complex, due to the scattering of light. Therefore, the band at  $\sim 585$  nm corresponds to the shiny complex (between cationic LDS 698 and anionic dodecyl sulphate (DS) ions), and the band at  $\sim 662$  nm corresponds to the monomer species entrapped in SDS micelles.

**3.2.2. Binding of LDS 698 with CT DNA.** In water, LDS 698 molecules show an absorption maximum at  $\sim 434$  nm. But gradual addition of CT DNA to the aqueous buffer solution leads to significant changes in the UV-vis spectrum. A decrease in the optical density value of LDS 698, along with a significant red shift in the absorption spectrum, is observed. In 1 mM CT DNA solution, the LDS 698 molecules show an absorption maximum at  $\sim 477$  nm. This kind of bathochromic shift indicates strong interactions between CT DNA and dye molecules.<sup>40,81</sup>

In the emission spectrum, enhancement in the fluorescence intensity is observed, along with a blue shift in the emission maximum, as the concentration of CT DNA in the aqueous

buffer solution increases. The observed fluorescence enhancement can be attributed to significant interactions between LDS 698 and DNA molecules. The variations in the absorption and emission profiles of LDS 698 are shown in Fig. 6. When LDS 698 binds to the DNA surface, it experiences a microenvironment that is more hydrophobic compared with aqueous buffer solution. As mentioned earlier, the LDS 698 molecules show a red shift in the absorption spectrum and a blue shift in the emission spectrum upon binding to hydrophobic species.<sup>73</sup> Therefore, this observation suggests that LDS 698 molecules bind to the DNA surface.

As the value of the binding constant provides information about the mode of binding between DNA and LDS 698 molecules, we calculated the binding constant between the two parties concerned using the following modified Benesi–Hildebrand<sup>82</sup> equation:

$$\frac{F_\infty - F_0}{F_t - F_0} = 1 + \frac{1}{K[C]} \quad (7)$$

Here,  $F_0$ ,  $F_t$  and  $F_\infty$  are the fluorescence intensities of LDS 698 in the absence of CT DNA, at various CT DNA concentrations, and at the point of saturation, respectively.  $[C]$  denotes the concentration of CT DNA, and  $K$  is the binding constant between CT DNA and LDS 698 molecules. The plot of  $\left(\frac{F_\infty - F_0}{F_t - F_0}\right)$  against  $[C]^{-1}$  shows a straight line and indicates a 1:1 interaction between the CT DNA and LDS-698 molecules (Fig. 7). This plot provides a binding constant of  $\sim 3.66 \times 10^3 \text{ M}^{-1}$ , which implies electrostatic interactions and minor groove binding of LDS 698 molecules, as the binding constant should have a much higher order of magnitude in the case of intercalation of the dye in the DNA base pairs.<sup>40,83</sup>

To obtain further information regarding the interaction of LDS 698 with micelles and DNA molecules, we performed isothermal titration calorimetric (ITC) measurements. The detailed experimental procedure and the ITC profiles of the dye with surfactant micelles or DNA are included in the ESI† (Fig. S2). The ITC profiles provide a qualitative idea about the interactions between the dye and the surfactant micelles or DNA molecules. From the ITC profiles, it is clear that the interaction between SDS and LDS 698 is stronger than that

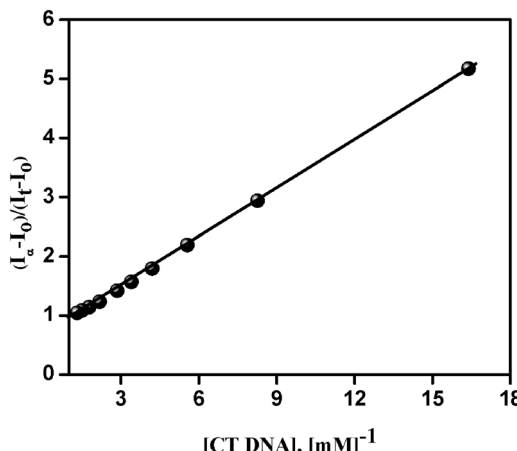


Fig. 7 Plot of  $(I_\infty - I_0)/(I_t - I_0)$  vs.  $[CT\ DNA]^{-1}$ .

between CT DNA and LDS 698 molecules, although both SDS and CT DNA are anionic.

### 3.3. Steady state fluorescence quenching study

Recently,  $\text{Cu}^{2+}$  ions have been used to monitor the fluorescence quenching of a probe molecule in pure aqueous solution, as well as in various biomimicking supramolecular assemblies.<sup>84,85</sup> This experiment also provides qualitative information regarding the location of the dye molecule and the protection efficiency of various supramolecular assemblies. Here, the fluorescence quenching of LDS 698 in micellar solutions was monitored using  $\text{Cu}^{2+}$  as a metal ion quencher, in order to investigate the ability of the quencher to access the probe in different micelles with different surface charges. The  $\text{Cu}^{2+}$  ion induced quenching constant of LDS 698 was calculated using the Stern–Volmer equation:<sup>69</sup>

$$\frac{I_0}{I} = 1 + K_{SV}[Q] \quad (8)$$

where  $I_0$  and  $I$  represent the fluorescence intensity of the fluorophore (LDS) in the absence and presence of quencher, respectively.  $[Q]$  is the concentration of the quencher ( $\text{Cu}^{2+}$ ), and  $K_{SV}$  is the Stern–Volmer quenching constant. A higher value of  $K_{SV}$  indicates greater exposure of the quencher to the probe molecules.

$\text{Cu}^{2+}$  ions are mainly present in water or in the polar Stern layer of micelles. In addition, the surface charge of the micelles is crucial in bringing  $\text{Cu}^{2+}$  to the Stern layer. The Stern–Volmer plots for  $\text{Cu}^{2+}$  and LDS 698 in water and various micelles are shown in Fig. 8. Fig. 8 clearly indicates that the quenching efficiency is a maximum for SDS micelles and a minimum for CTAB micelles. In SDS solution, the electrostatic attraction between the negative surface charge and the positive charge of the quencher ensures a close proximity between  $\text{Cu}^{2+}$  ions and LDS 698. In CTAB micelles, the quenching is least because of the repulsive interaction between the positive surface charges of CTAB and  $\text{Cu}^{2+}$  ions. This prevents the approach of  $\text{Cu}^{2+}$  in the Stern layer. In aqueous solutions of LDS 698, the electrostatic repulsion also prevents close approach between LDS 698 and  $\text{Cu}^{2+}$  ions.

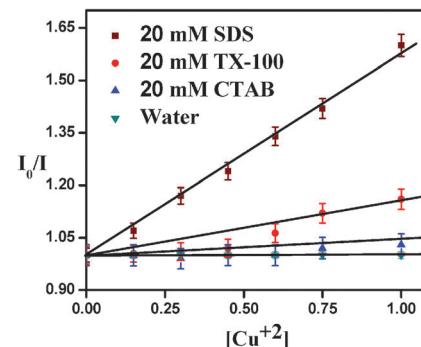


Fig. 8 Stern–Volmer plots for the steady state fluorescence quenching of LDS 698 by  $\text{Cu}^{2+}$  ions in water and micellar solutions of SDS, CTAB and TX-100.

### 3.4. Time resolved emission measurements

Time resolved measurements can provide more concrete information than steady state measurements in exploring the local environment around the probe molecules in organized assemblies.<sup>46,47,84,85</sup> The emission decays of LDS 698 in different micelle solutions are depicted in Fig. 9, and the corresponding fitting parameters are compiled in Table 3. In water, the fluorescence decay of LDS 698 is very fast and close to the instrument response function. So, the least squares fitting accompanied by deconvolution with a single exponential decay profile provided a time constant of  $\sim 36$  ps. Lifetime measurements depend on partitioning of the probe in homogeneous or heterogeneous phases and can provide important information regarding the location of dye molecules. Therefore, the modulated photophysics of the dye can be demonstrated using time resolved measurements.

Depending upon the partition of probe molecules in confined systems like micelles, vesicles or reverse micelles, differences in the lifetime measurement values are observed. In micellar solutions (SDS/CTAB/TX-100), the fluorescence decays are fitted with a bi-exponential function:<sup>69</sup>

$$f(t) = a_1 e^{-t/\tau_1} + a_2 e^{-t/\tau_2} \quad (9)$$

The fluorescence decay in micellar solution is quite slow compared to that in water. Successive addition of surfactant contributes to the bi-exponential nature of the emission decays (Fig. 9); for example, in 0.5 mM aqueous TX-100 solution, the lifetime components are  $\sim 38$  ps (99%) and  $\sim 677$  ps (1%). The shorter component is probably due to the presence of LDS 698 in the aqueous phase, and the longer lifetime component is assigned to entrapped LDS 698 in the micellar phase. Interestingly, with increasing concentration of surfactant, the relative contribution of the fast component decreases, which indicates the encapsulation of LDS 698 in the micellar phase. The decay parameters of LDS 698 in different surfactant solutions are given in Table 3. The solubilization of probe molecules in the micellar environment depends on its structure. In a micellar medium, the probe molecules may be solubilized in the Stern layer/palisade layer and the core of the micelles, in the

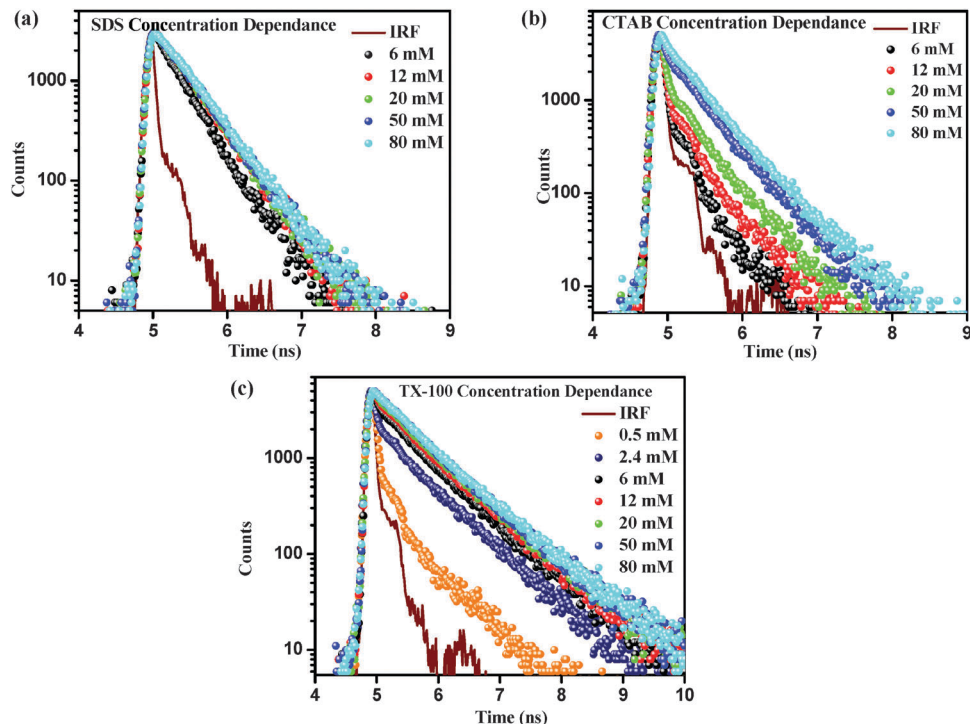


**Fig. 9** Time resolved fluorescence decay of LDS 698 in aqueous solutions of (a) SDS, (b) CTAB, and (c) TX-100 with increasing concentration ( $\lambda_{\text{ex}} = 408 \text{ nm}$ ).

**Table 3** Fluorescence quantum yields ( $\phi$ ), lifetimes ( $\tau$ ), and radiative ( $k_r$ ) and non-radiative ( $k_{nr}$ ) rate constants of LDS 698 in aqueous solutions with increasing concentrations of surfactant

System	Conc. (mM)	Quantum yield ( $\phi$ ) ( $10^{-2}$ )	$\tau_1 (a_1)$ (ps)	$\tau_2 (a_2)$ (ps)	$\langle \tau_{\text{av}} \rangle^a$ (ps)	$k_r (10^8 \text{ s}^{-1})$	$k_{nr} (10^9 \text{ s}^{-1})$	$\chi^2$
Water		0.110	36 (1.00)		36	0.305	27.747	1.13
SDS	6	0.261	109 (0.41) 120 (0.20) 129 (0.16) 129 (0.13) 136 (0.13)	329 (0.59)	239	0.109	4.173	1.08
	12	0.552		369 (0.80)	319	0.173	3.117	1.14
	20	0.573		381 (0.84)	340	0.168	2.924	1.15
	50	0.593		385 (0.87)	352	0.168	2.824	1.10
	80	0.621		390 (0.87)	357	0.174	2.784	1.07
CTAB	6	0.123	36 (0.98) 36 (0.97) 39 (0.94) 58 (0.73) 92 (0.54)	323 (0.02)	42	0.293	23.780	0.88
	12	0.153		375 (0.03)	46	0.333	21.706	0.85
	20	0.178		408 (0.06)	61	0.292	16.364	0.80
	50	0.353		418 (0.27)	155	0.228	6.429	0.86
	80	0.496		446 (0.46)	255	0.195	3.902	0.89
TX-100	0.5	0.127	38 (0.99) 54 (0.88) 92 (0.68) 153 (0.54) 225 (0.50) 274 (0.51) 294 (0.49)	677 (0.01)	44	0.289	22.698	0.85
	2.4	0.287		702 (0.12)	132	0.217	7.554	0.90
	6	0.505		714 (0.32)	291	0.174	3.419	1.16
	12	0.728		750 (0.46)	428	0.170	2.319	1.11
	20	0.841		791 (0.50)	508	0.165	1.952	0.95
	50	1.004		807 (0.49)	535	0.188	1.850	1.00
	80	1.058		815 (0.51)	560	0.189	1.767	1.12

<sup>a</sup> Experimental error ~6%.

interfacial region, or in bulk water. Neutral molecules are primarily solubilized in the Stern layer or the core of the micelle, and charged molecules are solubilized in bulk water or at the micelle–water interface. As LDS 698 is a cationic probe, it is anticipated that it is mainly solubilized in bulk water or at the micelle–water interface. But the experimental observations indicate that the lifetime components of LDS 698 in various

micellar media at different concentrations (Table 3) are higher than the component observed in water. Therefore, the results indicate that the probe molecules solubilize in two regions in the micellar environment. So, we can assign the longer lifetime component to probe molecules located in the Stern/palisade layer, and the other component is due to probe molecules located at the micelle–water interface or in bulk water. The pre-exponential

factors of the emission decays indicate that almost 50% of the probe molecules are solubilized in the Stern layer of CTAB and TX-100 solutions. But in SDS solution, almost 87% partition is observed in the micellar phase. This is due to attractive electrostatic interactions of cationic LDS 698 with anionic SDS surfactant. The increase in lifetime in different surfactant solutions with increasing concentration follows the trend: TX-100 > SDS > CTAB. As aqueous TX-100 solution offers greater microviscosity compared to the other surfactants, the maximum increase in the lifetime of LDS 698 is observed in TX-100 solution.

The LDS 698 molecule shows a single exponential decay pattern in aqueous solution, but with the addition of CT DNA, the time resolved emission decays deviate significantly from a single exponential nature to a complicated tri-exponential function (Fig. 10). Multi-exponential decay of dye molecules in the presence of DNA has also been reported in the literature.<sup>20,34</sup> But it is difficult to assign the exact location of dye molecules in DNA. LDS 698 is water soluble and therefore, the short component is likely to correspond to unbound LDS 698 molecules, and the other two components refer to the dye molecules bound to the DNA surface. Therefore, without

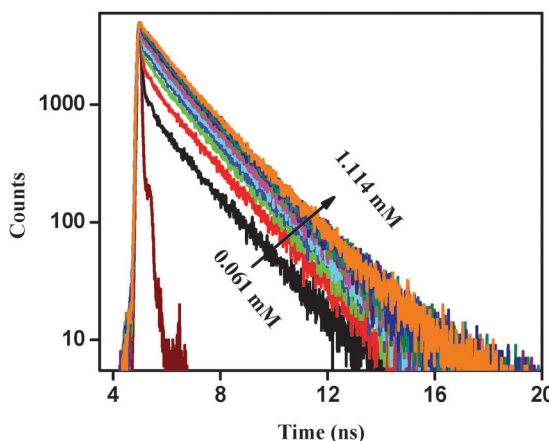


Fig. 10 Time resolved fluorescence decay of LDS 698 in aqueous solutions with increasing concentrations of CT DNA.

Table 4 Fluorescence quantum yields ( $\Phi$ ), lifetimes ( $\tau$ ), and radiative ( $k_r$ ) and non-radiative ( $k_{nr}$ ) rate constants of LDS 698 in aqueous solutions with increasing concentrations of Calf Thymus DNA (CT DNA)

System	Conc. (mM)	Quantum yield ( $\Phi$ ) ( $10^{-2}$ )	$\tau_1 (a_1)$ (ps)	$\tau_2 (a_2)$ (ps)	$\tau_3 (a_3)$ (ps)	$\langle \tau_{av} \rangle^a$ (ps)	$k_r (10^8 \text{ s}^{-1})$	$k_{nr} (10^9 \text{ s}^{-1})$	$\chi^2$
CT DNA	0	0.110	36 (1.00)			36	0.305	27.747	1.13
	0.061	0.350	40 (0.95)	623 (0.01)	1736 (0.04)	113.67	0.3079	8.7666	0.95
	0.121	0.551	44 (0.90)	701 (0.03)	1771 (0.07)	184.60	0.2985	5.4049	0.91
	0.180	0.740	44 (0.84)	706 (0.05)	1793 (0.11)	269.49	0.2746	3.6833	0.97
	0.238	0.932	45 (0.81)	706 (0.06)	1810 (0.13)	314.11	0.2967	3.1539	0.95
	0.294	1.110	48 (0.70)	711 (0.09)	1809 (0.21)	477.48	0.2325	2.0711	0.92
	0.350	1.301	48 (0.71)	745 (0.09)	1810 (0.20)	463.13	0.2809	2.1311	0.96
	0.458	1.503	60 (0.60)	745 (0.13)	1841 (0.27)	629.92	0.2386	1.5636	0.91
	0.562	1.700	60 (0.56)	760 (0.14)	1832 (0.30)	689.60	0.2465	1.4255	0.94
	0.759	1.988	63 (0.49)	772 (0.17)	1841 (0.34)	788.05	0.2523	1.2437	0.92
	0.852	2.022	66 (0.43)	778 (0.18)	1839 (0.39)	885.63	0.2283	1.1063	0.93
	0.943	2.108	66 (0.44)	780 (0.18)	1852 (0.38)	873.20	0.2414	1.1211	0.95
	1.114	2.200	68 (0.43)	785 (0.19)	1862 (0.38)	885.95	0.2483	1.1039	0.97

<sup>a</sup> Experimental error ~5%.

emphasizing individual components, we calculated the average lifetime using eqn (3), and the results are presented in Table 4. Careful observation of Table 4 reveals that the mean lifetime ( $\tau_{av}$ ) increases significantly with increasing CT DNA concentration. It is interesting that the relative component of the shorter lifetime in aqueous solution progressively decreases with the addition of CT DNA.

The change in the fluorescence lifetime of the probe molecules with successive addition of surfactant and CT DNA helps in estimating the radiative and non-radiative rate constants for entrapment in surfactant assemblies. We estimated the radiative ( $k_r$ ) and non-radiative ( $k_{nr}$ ) rate constants from the quantum yield ( $\Phi$ ) and the average fluorescence lifetime ( $\tau_{av}$ ) using the following equations:<sup>69</sup>

$$k_r = \frac{\Phi}{\tau_{av}} \quad (10)$$

$$k_{nr} = \frac{1}{\tau_{av}} - k_r \quad (11)$$

where  $k_r$  and  $k_{nr}$  represent the radiative and non-radiative rate constants, respectively. The calculated values are provided in Table 3 (for micelles) and Table 4 (for CT DNA). In pure water, the non-radiative rate constant is very high at  $\sim 27 \times 10^9 \text{ s}^{-1}$ , and similarly high non-radiative rate constants are also observed in other high polarity solvents.<sup>13</sup> Again, due to the possibility of photo-isomerisation, solvent viscosity also influences the non-radiative rate. In micellar medium and on the DNA surface, the probe molecules may experience lower polarity and higher microviscosity. Therefore, it is expected that the non-radiative rate constant should be lower compared with those observed in water or other polar solvents. The non-radiative rates in organized assemblies are  $\sim 2.784 \times 10^9 \text{ s}^{-1}$  (SDS),  $\sim 3.902 \times 10^9 \text{ s}^{-1}$  (CTAB),  $\sim 1.767 \times 10^9 \text{ s}^{-1}$  (TX-100) and  $1.1039 \times 10^9 \text{ s}^{-1}$  (CT DNA). According to the observed results, the non-radiative rate constant is higher in aqueous medium compared to restricted environments. The variations of the non-radiative rate constant with concentration of different surfactants and CT DNA are shown in Fig. S3 and S4 (ESI†). Thus, enhancements in the radiative lifetime and fluorescence quantum yield in micellar assemblies and on CT DNA

surfaces can be considered in connection with reduction of non-radiative decay channels.

### 3.5. Temperature dependent studies

It is believed that the torsional motion of cyanine dye molecules also depends on the temperature of the system. To examine the effect of the various microenvironments provided by surfactant and CT DNA on the non-radiative deactivation of LDS 698 at different temperatures, we recorded steady state and time resolved emission profiles in a temperature range between 283 K and 308 K (Fig. S5, ESI†). It is clear that the fluorescence intensity and the emission lifetime of LDS 698 decrease sharply with increasing solution temperature. The variation of the lifetime of LDS 698 with increasing temperature is provided in Table 5. To get an idea about the relative efficiencies of the microheterogeneous media of micelles and DNA for reducing the temperature induced non-radiative deactivation, we plotted  $\frac{\tau_{283}}{\tau_T}$  against temperature (Fig. 11). The average lifetimes of LDS 698 in SDS, CTAB, TX-100 and DNA surfaces were found to be  $\sim 559$  ps,  $\sim 512$  ps,  $\sim 814$  ps and  $\sim 1042$  ps, respectively at 283 K, and these values decreased to  $\sim 286$  ps,  $\sim 220$  ps,  $\sim 447$  ps and  $\sim 842$  ps, respectively at 308 K. Thus, with increasing temperature, the relative decreases in average lifetimes are  $\sim 49\%$  (SDS),  $\sim 57\%$  (CTAB),  $\sim 45\%$  (TX-100) and  $\sim 19\%$  (CT DNA). It was observed that the relative decrease in the fluorescence lifetime is maximum in the microenvironment of CTAB and minimum in the microenvironment provided by DNA molecules. Therefore, the torsional motion, *i.e.* non-radiative deactivation of

LDS 698 molecules is highly hindered in the DNA microenvironment in the temperature range between 283 K and 308 K.

### 3.6. Ability of surfactant molecules to relocate or release LDS 698 between micelles and DNA surface

Circular dichroism (CD) measurements clearly suggest that the structural aspects of CT DNA molecules remain almost unaltered in the presence of SDS. However in the presence of 10 mM TX-100 solution, the CD profile of CT DNA molecules shows small changes below the 250 nm range. This may be due to self-absorption of TX-100 molecules in this range, or pi-pi interactions between the aromatic ring of the surfactant and the nitrogen bases of the polynucleotide. In CTAB solution, precipitation and a remarkable change in the CD spectrum was observed on addition of CT DNA. It has already been reported in the literature that condensation is a widely accepted processes that occurs in CT DNA in the presence of cationic surfactant.<sup>62,63</sup> Therefore, the interactions of the dye molecules with CT DNA solution in the presence of CTAB were not investigated.

To observe the switching behavior of dye molecules between the DNA surfaces and TX-100 or SDS micelles, we recorded the UV-vis absorption and emission spectra of LDS 698 in the presence of surfactant and DNA. The steady state absorption and emission spectra (Fig. S6, ESI†) of LDS 698 molecules in 10 mM SDS solution remain unaltered after the addition of CT DNA. This present result clearly indicates that the probe molecules are preferentially bound to SDS micelles, even in the presence of CT DNA. The release of LDS 698 from CT DNA was observed with the addition of SDS to a CT DNA solution. The respective changes in the absorption and

**Table 5** Fluorescence quantum yields ( $\Phi$ ), lifetimes ( $\tau$ ), and radiative ( $k_r$ ) and non-radiative ( $k_{nr}$ ) rate constants of LDS 698 in different micellar solutions as a function of temperature

System	Temp. (K)	$\tau_1 (a_1)$ (ps)	$\tau_2 (a_2)$ (ps)	$\tau_3 (a_3)$ (ps)	$\langle \tau_{av} \rangle^a$ (ps)	$\chi^2$
100 mM SDS	283	433 (0.42)	650 (0.58)		559	1.02
	288	395 (0.56)	607 (0.44)		488	1.06
	293	260 (0.29)	418 (0.71)		372	0.95
	298	166 (0.22)	407 (0.78)		354	0.95
	303	122 (0.12)	348 (0.88)		321	0.92
	308	116 (0.12)	310 (0.88)		286	0.93
100 mM CTAB	283	285 (0.55)	789 (0.45)		512	1.10
	288	203 (0.55)	668 (0.45)		412	1.03
	293	177 (0.53)	563 (0.47)		358	1.00
	298	157 (0.57)	481 (0.43)		296	0.95
	303	140 (0.54)	400 (0.46)		260	0.90
	308	115 (0.52)	334 (0.48)		220	0.85
100 mM TX-100	283	412 (0.47)	1170 (0.53)		814	1.04
	288	363 (0.50)	1058 (0.50)		711	1.08
	293	348 (0.52)	950 (0.48)		637	0.98
	298	298 (0.49)	815 (0.51)		562	0.94
	303	253 (0.48)	709 (0.52)		490	0.96
	308	264 (0.53)	654 (0.47)		447	1.20
1 mM CT DNA	283	961 (0.17)	2042 (0.41)	98 (0.42)	1042	0.98
	288	929 (0.20)	2003 (0.40)	92 (0.40)	1024	1.00
	293	838 (0.17)	1884 (0.43)	89 (0.40)	988	0.99
	298	800 (0.22)	1862 (0.41)	83 (0.37)	970	0.90
	303	763 (0.21)	1772 (0.41)	77 (0.38)	916	0.95
	308	750 (0.24)	1707 (0.34)	72 (0.42)	842	0.89

<sup>a</sup> Experimental error  $\sim 5\%$ .

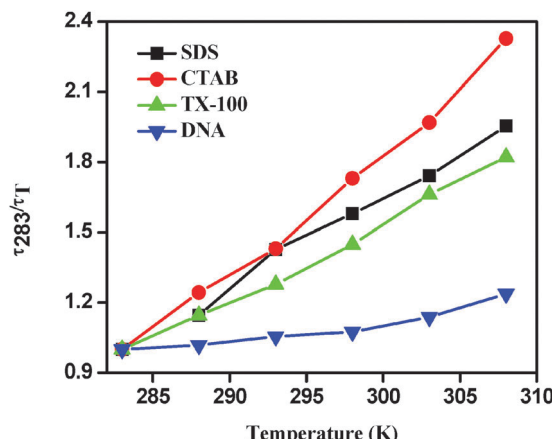


Fig. 11 Variation of the excited state lifetime of LDS 698 (relative to 283 K) ( $\frac{\tau_{283}}{\tau_T}$ ) with temperature in SDS, CTAB, TX-100 and CT DNA.

emission profiles are shown in Fig. 12. The emission intensity of a DNA-bound LDS 698 solution decreases significantly after addition of SDS above a particular concentration, due to the formation of a

non-fluorescent dye-surfactant complex. After the formation of a dye-bound micelle, the emission intensity increases again. The absorption and emission maxima are well correlated with the absorption and emission maxima of LDS 698 in SDS solution in the absence of DNA. Therefore, this result clearly shows that the probe molecules relocate from DNA surfaces to SDS micelles. To further verify this phenomenon, we measured the time resolved emission decays of LDS 698 in CT DNA solution with increasing SDS concentration (Fig. 12). In 1 mM CT DNA and 10 mM SDS solution, the fluorescence lifetimes of LDS 698 are  $\sim 884$  ps ( $\sim 68$  ps (43%),  $\sim 780$  ps (19%) and  $\sim 1860$  ps (38%)) and  $\sim 319$  ps ( $\sim 120$  ps (20%) and  $\sim 369$  ps (80%)), respectively. With the addition of SDS, the fluorescence lifetime of LDS 698 decreases due to the migration of probe molecules from DNA surfaces to SDS micelles. In 1 mM CT DNA solution containing 10 mM SDS, the fluorescence lifetime is  $\sim 392$  ps ( $\sim 180$  ps (13%) and  $\sim 448$  ps (87%)), which is very close to the lifetime of LDS 698 in aqueous SDS solution. Therefore, the absorption, emission and time resolved decays indicate that LDS 698 molecules are exclusively associated with SDS micelles in the presence of CT DNA.

We are now interested in observing the behavior of the probe molecules in TX-100 micelles with gradual addition of

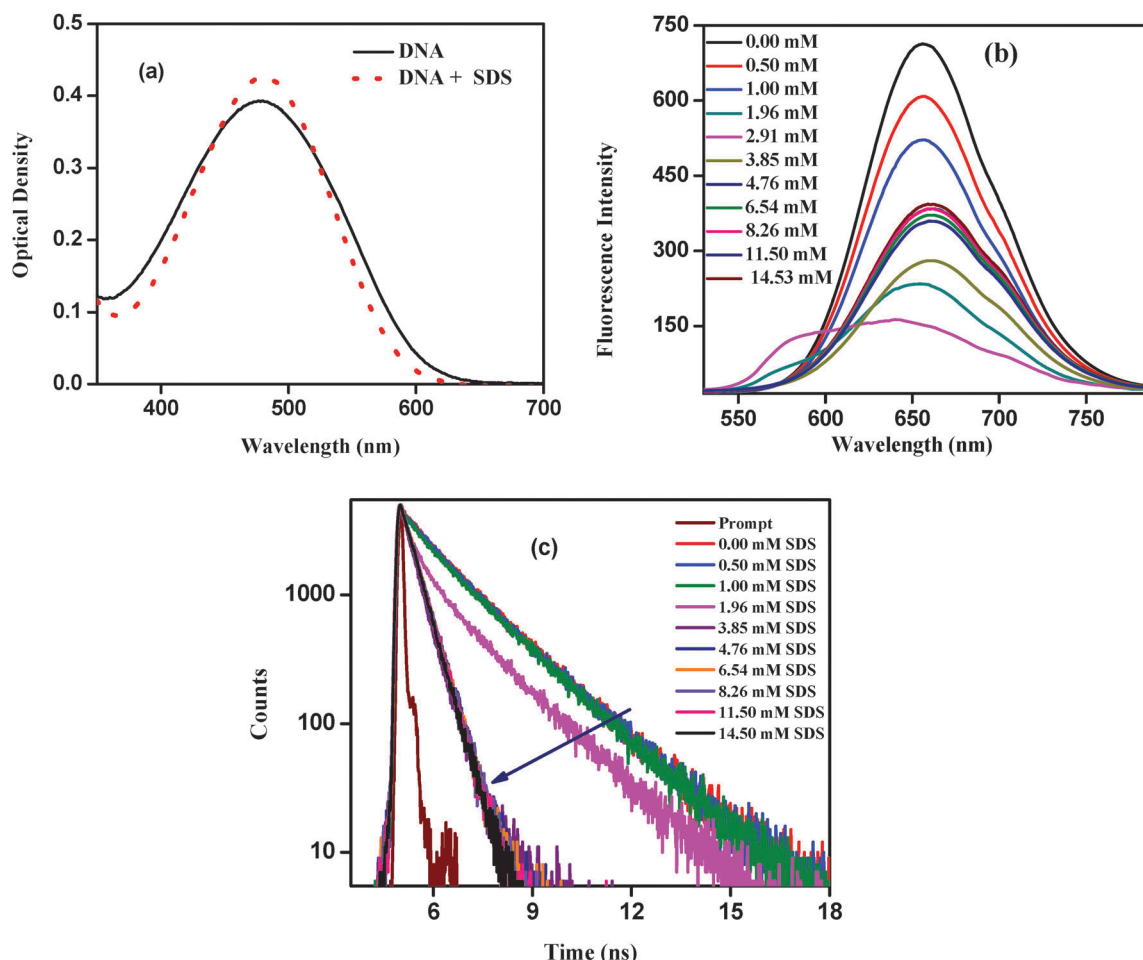


Fig. 12 Variation of (a) UV-vis spectral profiles, (b) emission profiles, and (c) fluorescence lifetimes of LDS 698 in 1 mM CT DNA solution with the addition of different concentrations of SDS.

CT DNA solution. In 10 mM aqueous TX-100 solution, LDS 698 shows an absorption band at  $\sim$  448 nm, which is gradually red shifted on addition of CT DNA solution. Similarly, an enhancement in the emission intensity with marginal red shift is observed in the fluorescence spectrum. The variation in the absorption and emission profiles of LDS 698 in TX-100 micelles with addition of CT DNA is shown in Fig. 13. To confirm the quantitative transfer of LDS 698 from TX-100 micelles to DNA surfaces, we recorded time resolved emission decays, and the results are shown in Fig. 13. In 10 mM TX-100 solution, the emission lifetime of LDS 698 is found to be  $\sim$  428 ps ( $\sim$  153 ps (54%) and  $\sim$  750 ps (46%)). But the decay becomes tri-exponential in nature on addition of CT DNA, and the fluorescence lifetime is  $\sim$  900 ps ( $\sim$  682 ps (34%),  $\sim$  86 ps (31%), and  $\sim$  1832 ps (35%)) in 10 mM TX-100 solution containing CT DNA. This is close to the lifetime of CT DNA in aqueous solution. Thus, the time resolved study further confirms the transfer of LDS 698 molecules from TX-100 micelles to DNA surfaces. The slight variation in the lifetime values of LDS 698 in both cases is due to changes in the bulk viscosity of the solution mixture in the presence of CT DNA and surfactant molecules.

We monitored the CD spectra of CT DNA with increasing temperature (Fig. S7, ESI<sup>†</sup>). The CD spectra clearly indicate that the secondary structure of CT DNA remains unchanged up to 343 K. Therefore, we performed temperature dependent UV-vis and fluorescence studies in CT DNA-LDS 698-SDS solution and in CT DNA-LDS 698-TX 100 solution in the temperature range from 298 K to 338 K. To compare the binding of LDS 698 with SDS and CT DNA, the same experiment was performed in CT DNA-LDS 698 solution and in SDS-LDS 698 solution. The UV-vis and fluorescence spectral changes are shown in Fig. S8 and S9 (ESI<sup>†</sup>). The variation of the fluorescence intensity ( $\frac{I_{298}}{I_T}$ ) with temperature (Fig. 14) provides further information regarding the interaction between LDS 698 and DNA in the presence of surfactant micelles. The ( $\frac{I_{298}}{I_T}$ ) versus  $T$  plots for SDS-LDS 698 solutions are the same in the absence and presence of CT DNA. This observation suggests that, in solutions containing CT DNA and SDS, the LDS 698 molecules are only strongly bound to SDS micelles. According to the CD spectra (Fig. S1e, ESI<sup>†</sup>), distortion in the secondary structure of DNA is observed

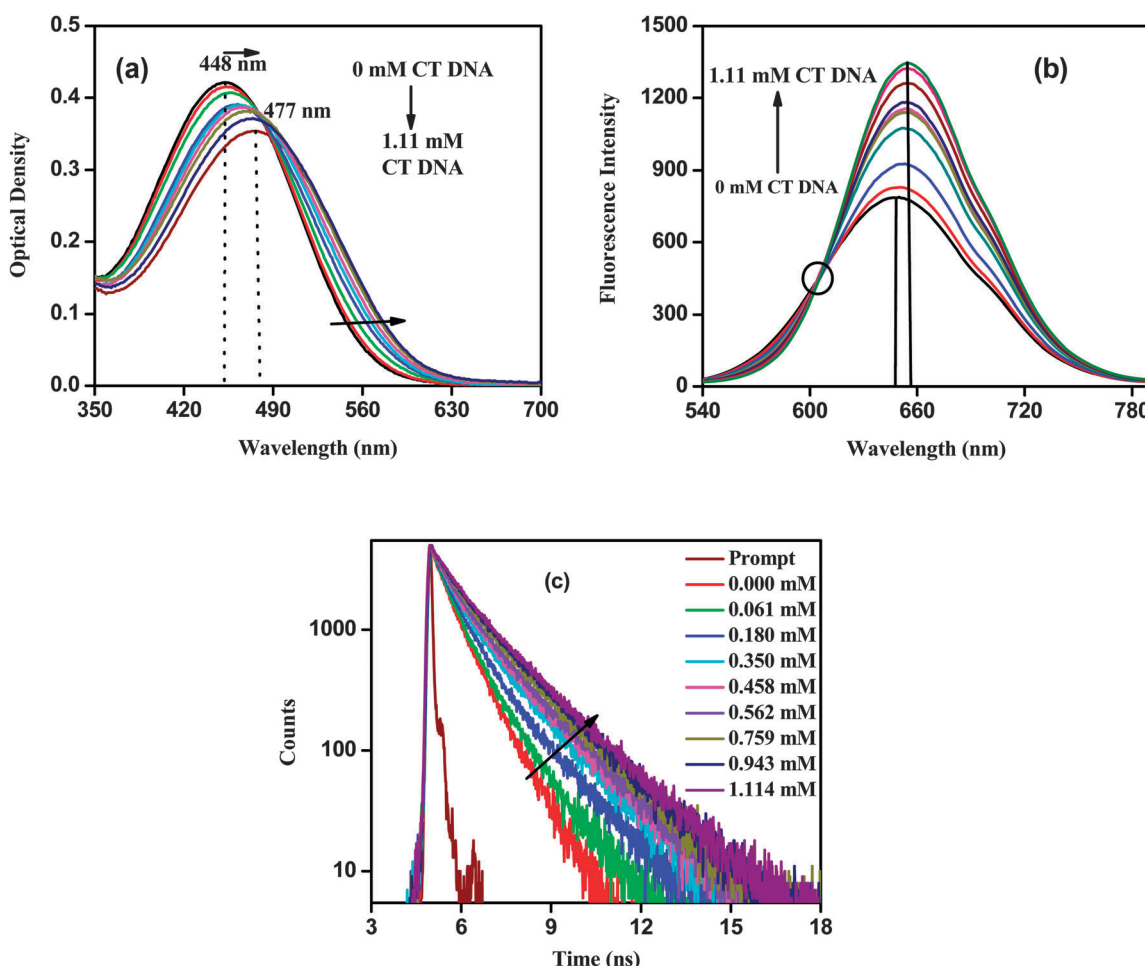


Fig. 13 Variation of (a) UV-vis spectral profiles, (b) emission profiles, and (c) fluorescence lifetimes decays of LDS 698 in 10 mM TX-100 solution with addition of different concentrations of CT DNA.

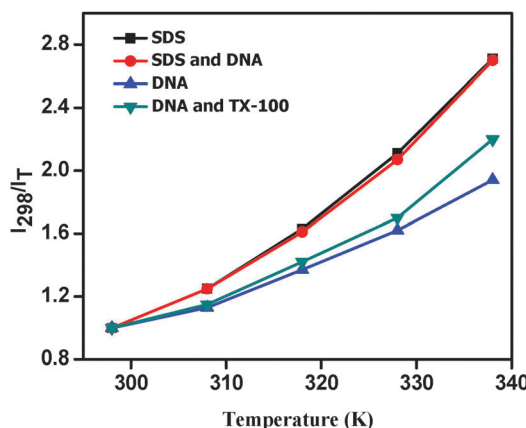


Fig. 14 Variation of fluorescence intensity of LDS 698 as a function of temperature in SDS and TX-100 solutions in the presence of CT DNA. For comparison, the variation of fluorescence intensity was also monitored in SDS and CT DNA solutions.

in the presence of TX-100. A deviation is also observed in the  $\left(\frac{I_{298}}{I_T}\right)$  against temperature plots for LDS 698 in CT DNA solution in the absence and presence of TX-100, although LDS 698 molecules are mainly associated with the DNA surface.

## 4. Conclusion

The present work demonstrates the interactions of a cationic hemicyanine dye with micelles with different surface charges, and with DNA. The interactions of the probe with organized assemblies are found to be dependant upon the charge, polarity and viscosity of the microheterogeneous environments. Due to the cationic nature of LDS 698, it is anticipated to be solubilized in bulk water or at the interface of the organized assemblies, but the results of the steady state and time resolved measurements indicate that a sufficient amount of the probe penetrates the Stern/palisade layer of the micelles and DNA surface. The interaction of the cationic probe with the anionic surfactant (SDS) results in the formation of pre-micellar aggregates or micelle-encapsulated monomers. These pre-micellar assemblies dissociate at higher surfactant (SDS) concentration. The presence of hydrophobic micelle and DNA environments around the probe reduces its twisting motion, resulting in an enhanced fluorescence quantum yield and lifetime. The observed decay lifetimes show that the emission can be increased in organized medium due to retardation of the twisting motion of the dye molecules. Further, we have investigated the specific interactions of probe molecules with micelles and DNA surfaces in a system containing both. Our investigation suggests that, in a solution containing SDS and DNA, LDS 698 interacts exclusively with the micelles, whereas in a solution containing TX-100, it preferentially releases from the micelles and relocates to the DNA surfaces. So, the present work demonstrates the interactions of a hemicyanine dye with biomimicking supramolecular assemblies of surfactant and DNA molecules, by monitoring its modified photophysics.

## Acknowledgements

N.S. is thankful to SERB, Department of Science and Technology (DST), Government of India, for generous research grants. S.G. and A.R. are thankful to CSIR for research fellowships. J.K. acknowledges UGC for a research fellowship. N.K. and D.B. are thankful to IIT Kharagpur for research fellowships.

## References

- E. Fluhler, V. G. Burnham and L. M. Loew, *Biochemistry*, 1985, **24**, 5749–5755.
- P. Fromherz and C. O. Müller, *Proc. Natl. Acad. Sci. U. S. A.*, 1994, **91**, 4604–4608.
- I. Lagadic, P. G. Lacroix and R. Clement, *Chem. Mater.*, 1997, **9**, 2004–2012.
- T. Coradin, R. Clement, P. G. Lacroix and K. Nakatani, *Chem. Mater.*, 1996, **8**, 2153–2158.
- O. M. Kostenko, V. B. Kovalska, K. D. Volkova, P. Shaytanov, I. O. Kocheshev, Y. L. Slominskiy, I. V. Pisareva and S. M. Yarmoluk, *J. Fluoresc.*, 2006, **16**, 589–593.
- X. M. Duan, H. Konami, S. Okada, H. Oikawa, H. Matsuda and H. Nakanishi, *J. Phys. Chem.*, 1996, **100**, 17780–17785.
- B. Strehmel, H. Seifert and W. Rettig, *J. Phys. Chem. B*, 1997, **101**, 2232–2243.
- H. Gorner and H. Gruen, *J. Photochem.*, 1985, **28**, 329–350.
- M. Panigrahi, S. Dash, S. Patel and B. K. Mishra, *J. Phys. Chem. B*, 2011, **115**, 99–108.
- J. Herbich, Z. R. Grabowski, H. Wojtowicz and K. Golankiewicz, *J. Phys. Chem.*, 1989, **93**, 3439–3444.
- J. L. McHale, *Acc. Chem. Res.*, 2001, **34**, 265–272.
- X. Cao, R. W. Tolbert, J. L. McHale and W. D. Edwards, *J. Phys. Chem. A*, 1998, **102**, 2739–2748.
- D. Seth, S. Sarkar, R. Pramanik, C. Ghatak, P. Setua and N. Sarkar, *J. Phys. Chem. B*, 2009, **113**, 6826–6833.
- P. Fromberz and A. Heilemann, *J. Phys. Chem.*, 1992, **96**, 6864–6866.
- R. Ramadass and J. Bereiter-Hahn, *J. Phys. Chem. B*, 2007, **111**, 7681–7690.
- N. C. Maiti, M. M. G. Krishna, P. J. Britto and N. Periasamy, *J. Phys. Chem. B*, 1997, **101**, 11051–11060.
- N. Nandi, K. Bhattacharyya and B. Bagchi, *Chem. Rev.*, 2000, **100**, 2013–2046.
- C. Ghatak, V. G. Rao, R. Pramanik, S. Sarkar and N. Sarkar, *Phys. Chem. Chem. Phys.*, 2011, **13**, 3711–3720.
- D. Ray, B. K. Paul and N. Guchhait, *Phys. Chem. Chem. Phys.*, 2012, **14**, 12182–12192.
- B. K. Paul and N. Guchhait, *J. Phys. Chem. B*, 2011, **115**, 11938–11949.
- D. Sarkar, P. Das, S. Basak and N. Chattopadhyay, *J. Phys. Chem. B*, 2008, **112**, 9243–9249.
- C. Martin, M. Gil, B. Cohen and A. Douhal, *Langmuir*, 2012, **28**, 6746–6759.
- M. Gil, M. Ziolk, J. A. Organero and A. Douhal, *J. Phys. Chem. C*, 2010, **114**, 9554–9562.
- K. Bhattacharyya, *Acc. Chem. Res.*, 2003, **36**, 95–101.

- 25 B. Jana, S. Senapati, D. Ghosh, D. Bose and N. Chattopadhyay, *J. Phys. Chem. B*, 2012, **116**, 639–645.
- 26 B. D. Wagner, *Phys. Chem. Chem. Phys.*, 2012, **14**, 8825–8835.
- 27 L. Valle, F. E. Morán Vieyra and C. D. Borsarelli, *Photochem. Photobiol. Sci.*, 2012, **11**, 1051–1061.
- 28 I. M. Verma and N. Somia, *Nature*, 1997, **389**, 239–242.
- 29 A. D. Miller, *Nature*, 1992, **357**, 455–460.
- 30 R. Acher, *Proteins and Nucleic Acids, Comprehensive Biochemistry*, Elsevier Publishing Company, New York, 1963, vol. 8.
- 31 S. E. Osborne and A. D. Ellington, *Chem. Rev.*, 1997, **97**, 349–370.
- 32 J. B. Chaires, *Curr. Opin. Struct. Biol.*, 1998, **8**, 314–320.
- 33 M. Gniazdowski and C. Cera, *Chem. Rev.*, 1996, **96**, 619–634.
- 34 I. Saha, M. Hossain and G. S. Kumar, *J. Phys. Chem. B*, 2010, **114**, 15278–15287.
- 35 D. M. Chenoweth and P. B. Dervan, *Proc. Natl. Acad. Sci. U. S. A.*, 2009, **106**, 13175–13179.
- 36 M. Foote-Zewail, *Anti-Cancer Drug Des.*, 1999, **14**, 1–9.
- 37 S. Murudkar, A. K. Mora, P. K. Singh and S. Nath, *Chem. Commun.*, 2012, **48**, 5301–5303.
- 38 W. Saenger, *Principles of Nucleic Acid Structure*, Springer-Verlag, New York, 1983.
- 39 A. Ianoul, F. Fleury, O. Duval, R. Waigh, J. C. Jardillier, A. J. P. Alix and I. Nabiev, *J. Phys. Chem. B*, 1999, **103**, 2008–2013.
- 40 D. Sahoo, P. Bhattacharya and S. Chakravorti, *J. Phys. Chem. B*, 2010, **114**, 2044–2050.
- 41 S. S. Maiti, S. S. Roy, S. Chall, S. Bhattacharya and S. C. Bhattacharya, *J. Phys. Chem. B*, 2013, **117**, 14655–14665.
- 42 G. Zhang, L. Wang, X. Zhou and D. Gong, *J. Agric. Food Chem.*, 2014, **62**, 991–1000.
- 43 Y. D. Ma, J. H. Pan, G. W. Zhang and Y. Zhang, *J. Photochem. Photobiol. B*, 2013, **126**, 112–118.
- 44 Y. D. Ma, G. W. Zhang and J. H. Pan, *J. Agric. Food Chem.*, 2012, **60**, 10867–10875.
- 45 N. Nandi, K. Bhattacharyya and B. Bagchi, *Chem. Rev.*, 2000, **100**, 2013–2045.
- 46 S. K. Pal, L. Zhao and A. H. Zewail, *Proc. Natl. Acad. Sci. U. S. A.*, 2003, **100**, 8113–8118.
- 47 S. K. Pal and A. H. Zewail, *Chem. Rev.*, 2004, **104**, 2099–2123.
- 48 K. Bhattacharyya, *Chem. Commun.*, 2008, 2848–2857.
- 49 N. Sarkar, K. Das, A. Datta, S. Das and K. Bhattacharyya, *J. Phys. Chem.*, 1996, **100**, 10523–10527.
- 50 S. Pal, S. Balasubramaian and B. Bagchi, *J. Chem. Phys.*, 2002, **117**, 2852–2859.
- 51 K. E. Furse and S. A. Corcelli, *J. Phys. Chem. Lett.*, 2010, **1**, 1813–1820.
- 52 J. D. Dignam, X. Qu, J. Ren and J. B. Chaires, *J. Phys. Chem. B*, 2007, **111**, 11576–11584.
- 53 P. K. Singh and S. Nath, *J. Phys. Chem. B*, 2013, **117**, 10370–10375.
- 54 A. Patra, S. Hazra, G. S. Kumar and R. K. Mitra, *J. Phys. Chem. B*, 2007, **111**, 11576–11584.
- 55 T. Shim, M. H. Lee, D. Kim and Y. Ouchi, *J. Phys. Chem. B*, 2008, **112**, 1906–9717.
- 56 Y. Huang, T. Cheng, F. Li, C. Luo and C. H. Huang, *J. Phys. Chem. B*, 2002, **106**, 10031–10040.
- 57 Y. Huang, T. Cheng, F. Li, C. H. Huang, T. Hou, A. Yu, X. Zhao and X. Xu, *J. Phys. Chem. B*, 2002, **106**, 10020–10030.
- 58 U. Narang, C. F. Zhao, J. D. Bhawalkar, F. V. Bright and P. N. Prasad, *J. Phys. Chem.*, 1996, **100**, 4521–4525.
- 59 H. Ephardt and P. Fromherz, *J. Phys. Chem.*, 1989, **93**, 7717–7725.
- 60 Q. Song, P. W. Bohn and G. J. Blanchard, *J. Phys. Chem. B*, 1997, **101**, 8865–8873.
- 61 *DNA Interactions with Polymers and Surfactants*, ed. R. S. Dias and B. Lindman, John Wiley & Sons, Inc., Hoboken, NJ, 2008.
- 62 J. Carlstedt, D. Lundberg, R. S. Dias and B. Lindman, *Langmuir*, 2012, **28**, 7976–7989.
- 63 E. Grueso, C. Cerrillos, J. Hidalgo and P. Lopez-Cornejo, *Langmuir*, 2012, **28**, 10968–10979.
- 64 M. Rosa, R. Dias, M. G. Miguel and B. Lindman, *Biomacromolecules*, 2005, **6**, 2164–2171.
- 65 B. Sohrabi, V. Khani, A. A. Moosavi-Movahedi and P. Moradi, *Colloids Surf. B*, 2013, **110**, 29–35.
- 66 J. P. Garcia, E. Marrón, V. I. Martín, M. L. Moyá and P. Lopez-Cornejo, *Colloids Surf. B*, 2014, **118**, 90–100.
- 67 S.-Y. Ran, Y.-W. Wang, G.-C. Yang and L.-X. Zhang, *J. Phys. Chem. B*, 2011, **115**, 4568–4575.
- 68 G. Jones, W. R. Jackson, C.-Y. Choi and W. R. Bergmark, *J. Phys. Chem.*, 1985, **89**, 294–300.
- 69 J. R. Lakowicz, *Principles of Fluorescence Spectroscopy*, Plenum, New York, 1999, vol. 2.
- 70 A. Bonincontro, M. Falivene, C. L. Mesa, G. Risuleo and M. R. Pena, *Langmuir*, 2008, **24**, 1973–1978.
- 71 B. A. Armitage, Cyanine dye-DNA, *Top. Curr. Chem.*, 2005, **253**, 55–76.
- 72 K. Shibasaki and K. Itoh, *J. Raman Spectrosc.*, 1991, **22**, 753–758.
- 73 D. Laage, W. H. Thompson, M. Blanchard-Desce and J. T. Hynes, *J. Phys. Chem. A*, 2003, **107**, 6032–6046.
- 74 M. Almgren, F. Grieser and J. K. Thomas, *J. Am. Chem. Soc.*, 1979, **101**, 279–291.
- 75 K. Weidemaier, H. L. Tavernier and M. D. Fayer, *J. Phys. Chem. B*, 1997, **101**, 9352–9361.
- 76 S. W. Snyder, S. L. Buell, J. N. Demas and B. A. DeGraff, *J. Phys. Chem.*, 1989, **93**, 5265–5271.
- 77 A. Mishra, R. K. Behera, P. K. Behera, B. K. Mishra and G. B. Behera, *Chem. Rev.*, 2000, **100**, 1973–2011.
- 78 A. S. Tatikolov and S. M. B. Costa, *Photochem. Photobiol. Sci.*, 2002, **1**, 211–218.
- 79 S. D. Choudhury, A. C. Bhasikuttan, H. Pal and J. Mohanty, *Langmuir*, 2011, **27**, 12312–12321.
- 80 N. C. Maiti, S. Mazumdar and N. Periasamy, *J. Phys. Chem. B*, 1998, **102**, 1528–1538.
- 81 F. A. Tanious, J. M. Veal, H. Buczak, L. S. Ratmeyer and W. D. Wilson, *Biochemistry*, 1992, **31**, 3103–3112.
- 82 H. A. Benesi and J. H. A. Hildebrand, *J. Am. Chem. Soc.*, 1949, **71**, 2703–2707.
- 83 S. Das and G. S. Kumar, *J. Mol. Struct.*, 2008, **872**, 56–63.
- 84 S. Mandal, V. G. Rao, C. Ghatak, R. Pramanik, S. Sarkar and N. Sarkar, *J. Phys. Chem. B*, 2011, **115**, 12108–12119.
- 85 B. K. Paul, D. Ray and N. Guchhait, *J. Phys. Chem. B*, 2012, **116**, 9704–9717.